Effect of Salicylate on the Elasticity, Bending Stiffness, and Strength of SOPC Membranes

Yong Zhou[†] and Robert M. Raphael[‡]
[†]Department of Biochemistry and Cell Biology, and [‡]Department of Bioengineering, Rice University, Houston, Texas

ABSTRACT Salicylate is a small amphiphilic molecule which has diverse effects on membranes and membrane-mediated processes. We have utilized micropipette aspiration of giant unilamellar vesicles to determine salicylate's effects on lecithin membrane elasticity, bending rigidity, and strength. Salicylate effectively reduces the apparent area compressibility modulus and bending modulus of membranes in a dose-dependent manner at concentrations above 1 mM, but does not greatly alter the actual elastic compressibility modulus at the maximal tested concentration of 10 mM. The effect of salicylate on membrane strength was investigated using dynamic tension spectroscopy, which revealed that salicylate increases the frequency of spontaneous defect formation and lowers the energy barrier for unstable hole formation. The mechanical and dynamic tension experiments are consistent and support a picture in which salicylate disrupts membrane stability by decreasing membrane stiffness and membrane thickness. The tension-dependent partitioning of salicylate was utilized to calculate the molecular volume of salicylate in the membrane. The free energy of transfer for salicylate insertion into the membrane and the corresponding partition coefficient were also estimated, and indicated favorable salicylate-membrane interactions. The mechanical changes induced by salicylate may affect several biological processes, especially those associated with membrane curvature and permeability.

INTRODUCTION

Salicylate, an active metabolite of aspirin and a popular non-steroidal anti-inflammatory drug (NSAID), has been used for centuries to treat fever, pain, and arthritis (1,2). The drug's main therapeutic function has been attributed to its ability to block the activity of cyclo-oxygenase (COX), which catalyzes the production of prostaglandin from arachidonic acid (2,3). Prostaglandins are important signaling molecules that regulate a number of biological processes and are important in the mammalian immune system. However, several of the main side-effects of salicylate and other NSAIDs are independent of tissue prostaglandin levels and appear not to be mediated by COX (1). These include effects on neutrophil aggregation (4), gastric intestinal (GI) toxicity (5,6), and reversible hearing loss (7,8). GI toxicity is especially noteworthy, because it leads to life-threatening ulcers. In the GI tract, gastric mucosal cells secrete phospholipids which form a hydrophobic barrier that protects the surrounding tissue from the acidic contents of the gut (5,9,10). Lichtenberger and co-workers have accumulated compelling evidence that the mechanism by which salicylate and related NSAIDs lead to ulcer formation is linked to the ability of these molecules to chemically associate with amphiphatic lipids and directly decrease the hydrophobicity of the mucus gel layer (6,11–13).

Consideration of salicylate's chemical structure suggests that salicylate will interact with phospholipids. Salicylate (α-hydroxybenzoic acid) is composed of a nonpolar benzene ring and a polar domain consisting of both carboxyl- and hydroxyl-functional groups (Fig. 1). This amphiphilic structure points to the likelihood that salicylate will penetrate into biomembranes and alter their physical properties. The consequences of salicylate's effects on membrane mechanics have not been characterized and quantified. Membrane mechanical properties are crucial to many cellular functions, such as permeability, shape deformation, adhesion, communication, fusion, and endo-/exocytosis. In addition, experimental evidence is accumulating that membrane elastic properties affect the function of integral membrane proteins, including the kinetics of ion channels (14).

Biomembranes are held together by hydrophobic forces, which give rise to surface tension (15,16). This cohesive force is opposed by a surface pressure, which balances with the surface tension in the stress-free condition. The difference between the surface tension and the surface pressure defines the membrane tension (17). Both surface tension and surface pressure are determined by lipid packing parameters, such as the surface area and molecular volume of the lipid headgroup and the length of the lipid acyl chain (18,19). When the membrane structure is perturbed by incorporation of amphiphilic molecules, such as salicylate, the lipid packing can be changed, thereby affecting lipid-lipid interactions.

The effects of a number of amphiphilic molecules on membrane mechanics have been investigated. For instance, short-chain alcohols (20,21), bile acids (22), and lysolipids (23) partition into the membrane and affect membrane elasticity, bending stiffness, and lysis tension. In the case of large surfactants, such as bile acids and lysolipids, the effects on the elastic compressibility were attributed to tension-dependent partitioning, i.e., the incorporation of more molecules into the membrane as the membrane is stretched by increases in applied pressure. In addition, small surfactants are predicted

Submitted November 18, 2004, and accepted for publication June 6, 2005.

Address reprint requests to Robert M. Raphael, Tel.: 713-348-3494; E-mail: rraphael@rice.edu.

0006-3495/05/09/1789/13 $2.00

doi: 10.1529/biophysj.104.054510

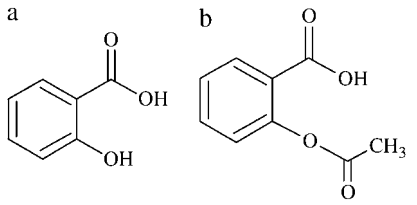

FIGURE 1 Chemical structures of salicylate (*a*) and aspirin (*b*) (ACD/ChemSketch 5.0). Both compounds are benzoic acid derivatives. Aspirin is quickly hydrolyzed to salicylate in an aqueous environment. These amphiphilic molecules interact with membranes, potentially leading to serious side effects.

to change the bilayer lateral pressure profile, leading to changes in membrane mechanical moduli and thickness (24). In this article we use micropipette aspiration of giant unilamellar lipid vesicles (GUVs) to characterize salicylate's ability to affect mechanical properties of a phosphatidylcholine (lecithin) membrane. We introduce a method to correct micropipette aspiration data for tension-dependent partitioning effects which is generally applicable to experiments with soluble surfactants. A quantitative understanding of the concentration dependence of salicylate's effects on membranes is important for ascertaining the drug's side effects in the physiological range.

We demonstrate that salicylate rapidly enters the membrane and reduces the apparent elastic area compressibility and bending moduli in a dose-dependent manner. Salicylate is especially effective at decreasing bending stiffness, although it has a smaller effect on the elastic area compressibility modulus, especially after accounting for the effects of tension-dependent partitioning. These changes are consistent with a salicylate-induced decrease in membrane thickness. The molecular volume of salicylate in the membrane is estimated to be $\sim$240 Å^3 by comparing the results of a transfer experiment to a ''sponge'' model developed by Evans et al. (22). The model is consistent with independent results that salicylate molecules exist as dimers in solution (25,26). We also estimated the free energy of transfer to be $\sim$13.5 kJ/mol and the corresponding partition coefficient to be $\sim$2.2 by converting our elastic compressibility moduli to surface-tension values (21). Taken together, the results verify that salicylate molecules prefer the membrane's hydrophobic environment over an aqueous one.

Finally, we explored the effects of salicylate on membrane strength by applying dynamic tension spectroscopy (DTS), a technique recently developed by Evans et al. (31). Membrane strength is indicated by the ability of the membrane to resist rupture under high values of applied tension. Evans et al. (31) propose that rupture of membrane is a molecular-dynamic process composed of two steps: an initial formation of a spontaneous defect followed by subsequent formation of an unstable hole (cavitation) that leads the membrane to burst. In this theoretical development, the terms ''defect'' and ''hole'' refer to energetic (or thermodynamic) states of the membrane, and do not necessarily correspond to a particular geometry. Under this scheme, the spontaneous defect represents a metastable state which can transition to an unstable hole that leads to membrane failure. Both of these processes have associated energy barriers, and the tension at which the membrane fails depends upon the rate of pressure loading because the rate of tension application changes the probability of the transition from a spontaneous defect to an unstable hole. DTS experiments reveal that salicylate increases the frequency of spontaneous defects and significantly lowers the tension scale for cavitation. The corresponding edge energy of the membrane hole calculated from the tension scale data indicates that salicylate stabilizes membrane holes.

Our mechanical and DTS measurements point to a unified picture in which the primary mechanical result of salicylate partitioning at low concentrations is a reduction in the membrane's bending stiffness. Many undesirable side effects of salicylate could stem from these mechanical effects on the membrane.

MATERIALS AND METHODS

Materials

The phospholipid 1-stearoyl-2-oleoyl-phosphatidyl-choline (SOPC) was purchased from Avanti Polar Lipids (Alabaster, AL). Lipids were dissolved in chloroform and stored at -20°C under nitrogen. Sodium salicylate and bovine serum albumin (BSA) were purchased from Sigma-Aldrich (St. Louis, MO). Glucose and sucrose were purchased from Fisher Scientific (Pittsburgh, PA).

Methods

Vesicle formation

Vesicles were formed from SOPC using an electroformation procedure (27,28). The SOPC/chloroform solution was spread on platinum electrodes aligned parallel and $\sim$5 mm apart from each other in a vesicle-making chamber. The chamber was then placed in a desiccator under vacuum for at least 2 h to ensure complete evaporation of chloroform. The dried lipid film was then slowly rehydrated in 200 mM sucrose solution. An alternating AC field with amplitude from 0.5 V to 2 V and frequency from 10 Hz to 1 Hz was then applied to the electrodes. After $\sim$2 h, SOPC vesicles with sizes between 10 μm and 40 μm in diameter would form and bud off the platinum electrodes. The vesicle solution was then collected in a glass vial and stored at 4°C under nitrogen.

We also formed SOPC GUVs using the traditional rehydration method (29) to ensure that the lipids were not oxidized during the electroformation process. Approximately 25 μl of 0.5 mg/ml SOPC/chloroform was spread on the roughened surface of a Teflon disk and dried under vacuum in a desiccator for at least 2 h. The Teflon disk with SOPC was rehydrated in 200 mM sucrose solution under N_2 overnight.

Micropipette aspiration

Microaspiration measurements were conducted on the stage of a Zeiss Axiovert 200M inverted microscope equipped with differential interference contrast (DIC) optics. We found that superior optical quality was achieved by using a Zeiss Plan-Neofluar 40×/0.85 polarized DIC objective (Carl

Zeiss, Thornwood, NY). Additional magnification was provided by a 1.6 optovar. Micropipettes used to apply pressure on lipid vesicles were fabricated using a micropipette puller (Sutter P-97, Novato, CA) and then broken cleanly on a custom-made microforge. A 0.02% bovine serum albumin (BSA) solution was then used to coat the pipette. An extensive washing of the coated pipette with both 200 mM glucose solution and distilled water was performed in an effort to eliminate excess BSA on the pipette (30).

The finished pipette with diameter of 8–10 μm was mounted on a micromanipulator coupled to a water-filled reservoir and inserted into the aspiration chamber that contains lipid vesicles suspended in isomolar glucose/salicylate solution (200 mOsM). Pressure loading was achieved by changing the height of a water column mounted on a motorized mechanical slider purchased from Robocylinder (RCP-SA6I-L-600-P, Torrance, CA). The pressure level was calibrated and periodically checked using small vesicular debris that was found in the chamber and was small enough (~1–2 μm in diameter) to move freely through the aspirating pipette. Unilamellar vesicles with a diameter between 18 μm and 40 μm were chosen for experiments. When negative pressure was applied, a portion of the vesicle would enter the pipette, creating a vesicular projection (Fig. 2 *a*). After each pressure-loading step, the vesicle was given at least 10 s for salicylate exchange to equilibrate between the vesicle and the bulk solution. This time was chosen because a transfer experiment (fully described below) used to characterize the timecourse of salicylate uptake indicated that it took <10 s for salicylate to complete its uptake into membrane (Fig. 3). After the projection length reached steady state, aspiration images were captured using a Zeiss Axiocam MRm camera. The vesicle and pipette dimensions were measured and analyzed using Zeiss Axiovision 3.0 software. To obtain accurate measurements of the projection length and the sizes of the pipette and vesicle, comparative light intensity plots (31) of the corresponding vesicle images were periodically used to verify the measurements obtained from the scaling software (Fig. 2 *b*). All measurements were conducted at room temperature and at the original pH of the salicylate/glucose solution. The pH was not manipulated for the concern that additional ions could complicate the results.

The following equations were applied to calculate membrane tension (τ) and apparent fractional area change (α_{app}) (32,33),

$$\tau = \frac{(P_o - P_p)R_p}{2(1 - R_P/R_v)}, \quad (1)$$

$$\alpha_{app} = \frac{\Delta A}{A} = \frac{2\pi R_p \Delta L(1 - R_p/R_v)}{4\pi R_v^2 - \pi R_p^2 + 2\pi R_p L}, \quad (2)$$

where A is membrane surface area; ΔA is the change in membrane area resulting from tension; R_v and R_p are radii of the aspirated vesicle and pipette, respectively; L is the vesicle projection length; and ΔL is the change in L resulting from the change in tension. Membrane tension (τ) was then plotted against the fractional area change (α_{app}). As shown in Fig. 4 *a*, a typical plot of τ versus α_{app} is composed of two regions. An initial exponential domain corresponds to low values of applied tension (<0.5 mN/m). In this area the work of the applied tension is predominantly used to decrease the thermally driven out-of-plane fluctuations of the membrane surface (34). This is the reason that the geometrically measured area expansion is designated as an apparent area change. Thermal fluctuations in vesicle shape are observed at room temperature because the bending energy is small and comparable to the thermal energy k_BT, where k_B is the Boltzmann constant and T is temperature in Kelvin (35). As the fluctuations are smoothed, the τ versus α_{app} curve makes a transition to a region of linear elastic behavior. The slope of the high-tension domain (>0.5 mN/m) is the apparent compressibility modulus, K_{app} (32,33). The initial low-tension region of the plot can be used to calculate the bending modulus k_c. Specifically, the slope of the low-tension portion of a plot of ln (τ) versus α_{app} (Fig. 4 *b*) is equal to $8\pi k_c/k_BT$ (34).

Elastic area compressibility modulus (K_A)

The thermodynamic compressibility modulus characterizes the energy associated with changing the area of the membrane. However, in the aspiration experiments, membrane thermal fluctuations are present throughout the entire tension range, causing the measured membrane area dilation to have contributions from smoothing thermal undulations at all tension levels (34). To obtain the elastic compressibility modulus, denoted K_A, the fractional area increase resulting from smoothing of membrane fluctuations

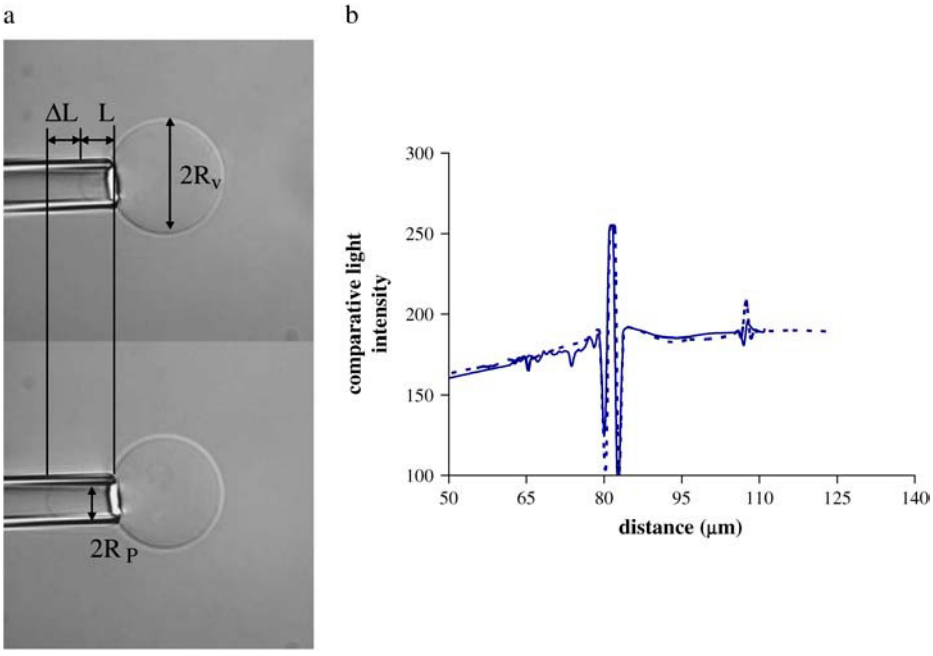

FIGURE 2 (*a*) DIC images of an aspirated SOPC vesicle at a low tension of 0.01 mN/m (*top*) and a higher tension of 7.3 mN/m (*bottom*). (*b*) Plots of comparative light intensity of the corresponding vesicle images in *a*. Using the Zeiss Axiovision 3.0 software, the light intensity values of the images along a horizontal line drawn across the center the pipette and vesicle were obtained. These light intensity data were then plotted against distance to indicate the exact location of the edges of the projection inside of the pipette and the tip of the pipette, as well as the edge of the vesicle outside of the pipette. The solid line represents the light intensity pattern at 0.01 mN/m, and the dotted line is the pattern at 7.3 mN/m. The small dip of the solid line at ~74 μm indicates the edge of the projection in the pipette. The huge variation at ~80 μm represents the tip of the pipette, where diffraction caused large variations in light intensity. The dip at ~110 μm is the edge of the vesicle outside of the pipette. The dotted line clearly shows that increasing the tension caused an increase in the projection length inside of the pipette.

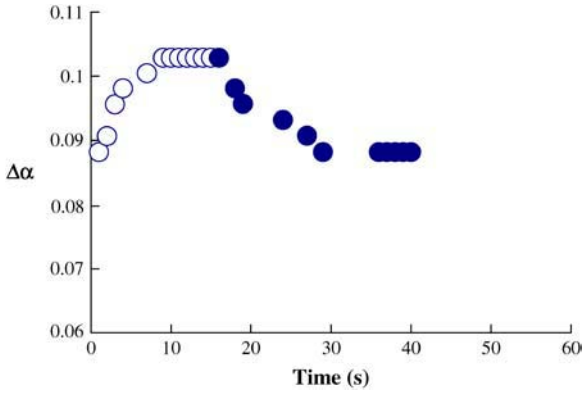

FIGURE 3 Kinetics of salicylate-membrane interaction. The timecourse of salicylate uptake into a SOPC vesicle suspended in 10 mM salicylate was obtained via the modified transfer experiment discussed in the text (for this vesicle, the tension was ~3.5 mN/m). The open circles indicate the uptake process. As shown, it took ~8 s for salicylate and lipids to equilibrate. The solid circles demonstrate when salicylate was removed, the projection length returned to its original position. The complete recovery took ~20 s. Both the original and modified transfer experiments give very similar results for the timecourse of salicylate uptake (data of the original transfer experiments not shown).

at each data point i was removed from the measured total area using the model developed by Evans and Rawicz (34) and Rawicz et al. (33). The removed fractional area increase, denoted $\Delta\alpha(i)$ is equal to

$$\Delta\alpha(i) = (k_BT/8\pi k_c)\ln[\tau(i)/\tau(1)], \quad (3)$$

where τ (1) is initial tension. The tension data for each vesicle was then replotted against the elastic area dilation, denoted α_A, where $\alpha_A(i) = \alpha_{app}(i) - \Delta\alpha(i)$. The elastic area compressibility modulus (K_A) is the slope of the τ-versus-α_A plot. K_A will always be larger than K_{app} because the total amount of $\Delta\alpha(i)$ increases with increasing tension, meaning that the slope of the plot of τ versus α_A is greater than that of τ versus α_{app}.

Transfer experiment

Soluble amphiphiles also complicate the calculation of the actual thermodynamic compressibility modulus. The uptake of a soluble amphiphile into the membrane is a complex kinetic process (23,36). When performing micropipette experiments with soluble amphiphiles, it is important to know whether the given amphiphile reaches equilibrium in the membrane and how long the approach to equilibrium takes. Moreover, important experimental parameters related to tension-dependent partitioning can be derived from these experiments. Salicylate incorporation into the membrane can be measured from the increased projection length of an aspirated vesicle exposed to salicylate. The transfer experiments were first conducted following previously described methods (36,37). Briefly, a chamber containing 200 mOsM glucose (the control chamber) was set side-by-side with another chamber filled with salicylate-glucose solution at the same osmolarity (200 mOsM) on the aspiration stage. Another, much larger micropipette (transfer pipette with diameter of at least 50 μm) containing control solution (200 mM glucose) was inserted into the chamber from the opposite side of the aspirating pipette. An aspirated vesicle was then inserted into the transfer pipette in the control chamber. The entire apparatus was moved to the salicylate chamber containing glucose-salicylate solution. The timecourse of the projection increase was recorded and converted to α_{app}, and the approach to equilibrium took <10 s. However, we were unable to record the recovery using this standard transfer process. We attribute this to the fact that the transfer pipette contains control solution, and the vesicle projection reaches equilibrium during the transfer process. Thus, the transfer experiment was modified.

The modified transfer experiment utilized the same dual-chamber setup as described above. However, the transfer pipette and the water column linked to the pipette were filled with a salicylate solution, instead of a control solution. The pressure in this pipette (the salicylate pipette) was then calibrated and set to zero in a chamber containing the same salicylate solution (the salicylate chamber). The manipulators holding the two pipettes were prealigned so that a rapid movement of the transfer pipette would place it exactly in front of the vesicle pipette. During the uptake experiment, the salicylate pipette was swiftly moved into the control chamber, the vesicle was inserted ~50-μm deep into the salicylate pipette and the timecourse of the projection length increase was recorded (Fig. 3). To monitor the projection length recovery, the salicylate pipette was swiftly moved back into the salicylate chamber and the recovery timecourse was recorded. The complete recovery of the vesicle projection in 200 mM glucose (Fig. 3) indicates that the residual salicylate in the control chamber was insignificant. This is expected due to the small volume of solution in the pipette as compared to the large volume of solution in the chamber. To prevent salicylate accumulation in the control chamber, solutions were changed frequently.

Tension dependence of salicylate partitioning

In addition to determining the timecourse of salicylate uptake, the transfer experiments can also be utilized to study the concentration- and tension-dependence of salicylate partitioning. During an aspiration experiment, the

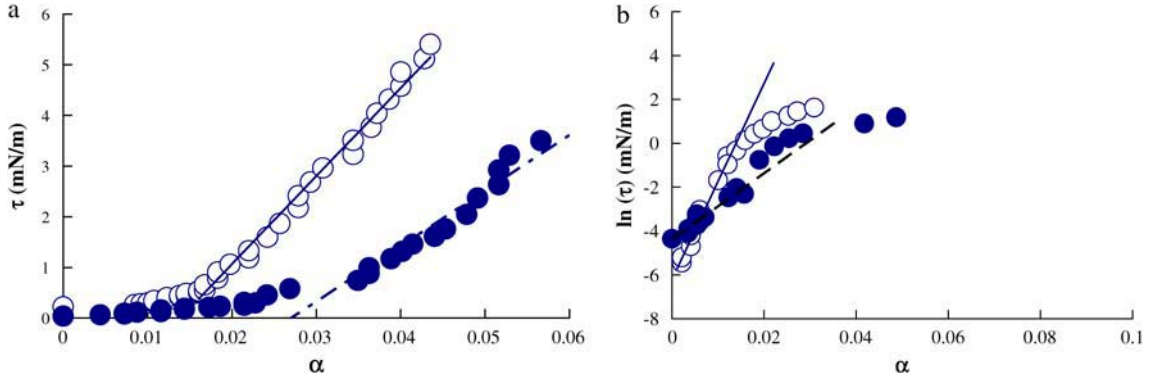

FIGURE 4 (*a*) Plot of tension (τ) versus fractional area change (α) for a representative vesicle. The slope of the high tension region (>0.5 mN/m) is the apparent area compressibility modulus (K_{app}). (*b*) Plot of ln (τ) versus α for another vesicle in which α in the low-tension region was carefully measured. The slope of the low-tension domain of the plot was used to calculate the bending modulus (k_c). Plots shown are SOPC in 200 mM glucose (○) and in 10 mM salicylate solution at 200 mOsM (●).

membrane is stretched and more salicylate partitions into the membrane, making the salicylate concentration in the membrane tension-dependent. In the extreme limit, K_A could vary as a function of tension. Hence the experimentally determined area dilation, $\alpha_{app}(i)$, at i^{th} tension level will contain a contribution from tension-dependent partitioning of salicylate molecules, designated $\alpha_{par}(i)$. To account for this, we define a term, $\alpha_{Ae}(i)$, which is the actual area increase caused by changes in lipid-lipid cohesion,

$$\alpha_{Ae}(i) = \alpha_{app}(i) - \alpha_{fl}(i) - \alpha_{par}(i), \tag{4}$$

where $\alpha_{fl}(i)$ is the area increase caused by smoothing of membrane fluctuations.

Thermodynamic theories developed for exchange of surfactants with bilayers can be used to obtain $\alpha_{par}(i)$. At equilibrium, the chemical potential of salicylate in the membrane is equal to that in the bulk solution (21,22),

$$\frac{1}{n_s}\ln\left(\frac{x_s}{n_s}\right) + \frac{\mu_s^o}{kT} = \frac{\mu_m^o}{kT} + \frac{1}{n_m}\ln\left(\frac{x_m}{n_m}\right) - \frac{\tau}{l_c}\frac{V_{sal}}{2kT}, \tag{5}$$

where μ_s^o and μ_m^o are the standard chemical potentials in the solution and inside of the membrane; x_s and x_m represent the mole fractions of the salicylate in solution and in vesicle membrane; V_{sal} is the molecular volume of the salicylate in the membrane; τ is the membrane tension; and l_c is the length of the hydrophobic core (estimated to be ~3 nm) (21). The term τ/l_c is the lateral pressure, whereas the terms n_s and n_m correspond to the number of salicylate molecules in aggregates inside and outside of the membrane; and are included because salicylate has been shown to form dimers in solution (25,26).

Eq. 5 indicates that the size of the salicylate molecule in the membrane will be the operative parameter in determining α_{par}. V_{sal} can be experimentally determined from the modified transfer experiment described earlier. An aspirated vesicle in the control solution was transferred into the salicylate pipette at different constant tension levels. The projection length change before and after the transfer at each tension was recorded and converted to fractional area changes. Because salicylate decreases k_c (see Experimental Results, below), the uptake of salicylate will add area by increasing membrane thermal undulations. We then removed the area increase associated with membrane undulations to obtain the area increase at a fixed tension level i caused only by salicylate partitioning, designated $\alpha_{par}(i)$.

Dynamic tension spectroscopy (DTS)

Traditionally, the strength of membranes has been studied by measuring the tension at which the membrane bursts, referred to as the lysis tension (29,38,39). However, the process of membrane lysis is complex. A recently developed technique, dynamic tension spectroscopy (DTS), has been used to explore the intricacies of salicylate's effects on membrane lysis. The rupture process of membranes consists of two steps: spontaneous defect formation followed by cavitation (hole) formation (31). Each process is characterized by a frequency of occurrence (ν) and an associated tension scale (σ). Experimentally four parameters are obtained from DTS: the tension scales of defect and cavitation formation, σ_δ and σ_c, and the frequencies of defect and cavitation processes, ν_δ and ν_c.

We have implemented this technique, described in detail by Evans et al. (31), in our laboratory. Briefly, using the same microaspiration setup, the motorized mechanical slider was used to apply pressure at various slider speeds. The entire experiment from the beginning to rupture was video-recorded using a CCD camera (Panasonic WV-BL204, Panasonic/Matsushita, Secaucus, NJ). The video file was later converted into image frames using X Video Converter (AoA Media, http://www.aoamedia.com) to determine the time at which the membrane burst. The pressure loading rate, R_σ, was calculated from the slope of the plot of membrane tension versus time (Fig. 5 *a*). The similar loading rate values (±0.5 mN/m/s) were grouped into bins and corresponding rupture tension measurements were averaged. Fig. 5 *b* shows a plot of $\tau_{rupture}$ versus $\log(R_\sigma)$, referred to as a DTS spectrum (31). When all data points were plotted, a very similar pattern to the plot obtained from the averaged data was seen. For the purpose of clarity, the averaged plot was used. Two distinct sections are present in the plot, a low-tension domain and a high-tension domain. The nonlinear, low tension domain represents the energy barrier for cavitation, or pore formation. The linear, high-tension domain represents the energy barrier for forming a spontaneous defect in the membrane. The two domains are described by the following two equations, respectively,

$$\sigma/\sigma_\delta \approx \mathrm{Log}_e(R_\sigma/\nu_{O\delta}\sigma_\delta), \tag{6}$$

$$-\sigma_c/\sigma + \log_e[\sigma/\sigma_c)^{5/2}/(1+\sigma/2\sigma_c)] \approx Log_e(R_\sigma/\nu_c\sigma_c). \tag{7}$$

The above equations were derived from the Markov master equations used to describe the development of membrane rupture (31). Equation 6 applies to spontaneous defect formation, and Eq. 7 governs cavitation formation. In a DTS spectrum, the slope of the linear high-tension domain (loading rates of >10 mN/m/s) is σ_δ and the extrapolation of the slope line can be used to calculate ν_δ because $R_\sigma^o = \nu_\delta\sigma_\delta$ (31). The parameters associated with cavitation, σ_c and ν_c, can be obtained by using Eq. 7 to fit the nonlinear, low-tension domain from the loading rates of 0.01 mN/m/s to 3 mN/m/s (31).

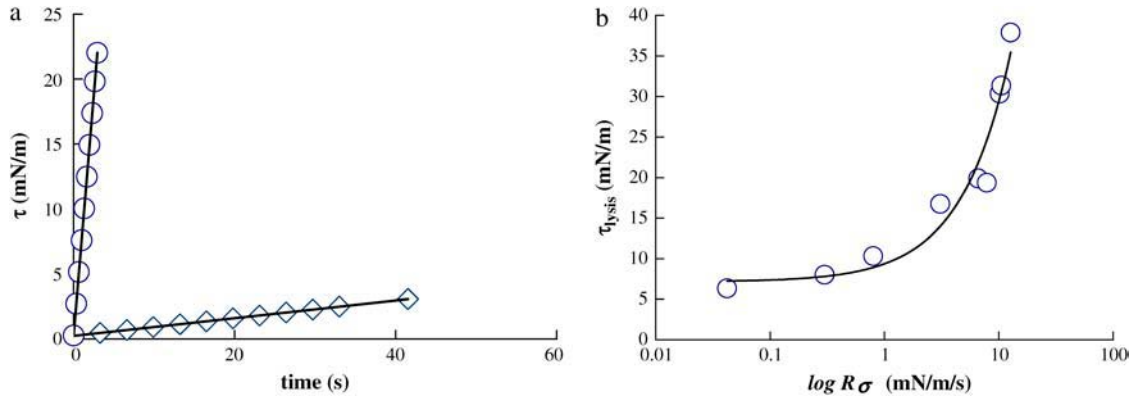

FIGURE 5 (*a*) Dependence of membrane rupture on loading rate. The results of experiments on two separate vesicles are shown. The pressure loading rate (R_δ) is the slope of the plot of membrane tension versus time. The experiment was carried out until membrane rupture. For the lower plot, vesicle rupture occurred at a tension 3 mN/m when $R_\delta = 0.068$ mN/m/s. For the upper plot, vesicle rupture occurred at 22 mN/m for $R_\delta = 7.4$ mN/m/s. The results clearly indicate that the tension needed to lyse a vesicle increases as R_δ increases. (*b*) A dynamic tension spectrum (*DTS*) of membrane rupture shows two distinct regions. The low-tension regime represents cavitation formation, whereas the high-tension regime indicates defect formation. For SOPC, σ_δ of defect formation is 3.2 mN/m and σ_c of cavitation is 197 mN/m.

BSA affects salicylate-membrane interactions

Bovine serum albumin (BSA) is traditionally used in microaspiration experiments to discharge the glass pipette surface (20,29,30). Initially, we performed control experiments with SOPC in 200 mM glucose with 0.02% BSA and found our data of K_{app} to be within the acceptable range for SOPC (~180 mN/m) and to be reproducible (mean ± SD of ~16 mN/m for 10 vesicles). Moreover, the measured values of K_{app} decreased in a dose-dependent manner in high concentrations of salicylate (>5 mM; data not shown). However, at low salicylate concentrations (<1 mM), the measurements were irreproducible. Previous investigators have reported that albumin binds to lipids and prevents membrane leakage (40). Shoemaker and Vanderlick (30) reported that elastic measurements of anionic vesicles were highly variable in the presence of BSA. Furthermore, sodium salicylate binds to BSA in solution and prevents heat coagulation of albumin molecules (41). Therefore, we decided to eliminate BSA in the aspiration chamber and only coat the glass pipette tip and coverslips of the chamber with 0.02% BSA and wash extensively with glucose solution and Millipore water, as discussed by Shoemaker and Vanderlick (30). When conducting studies without BSA in the system, all data became reproducible.

EXPERIMENTAL RESULTS

Apparent area compressibility measurements

We first measured the effect of salicylate on the apparent compressibility modulus of the membrane. A linear behavior in the high-tension domain (>0.5 mN/m) of the plot τ versus α_{app} demonstrates that the membrane still behaved as linear elastic material in the presence of salicylate. Fig. 6 shows that salicylate decreased K_{app} of SOPC in a dose-dependent manner. The range of salicylate concentrations tested was chosen to be 0.5–10 mM. The physiological effects of salicylate resulting from normal aspirin consumption occur at concentrations between 0.1 and 2 mM (42). When the blood serum level of salicylate reaches 10 mM, diverse pathological effects occur, including myocardial necrosis (43). The minimum amount of salicylate required to change the apparent membrane compressibility (K_{app}) was ~1 mM.

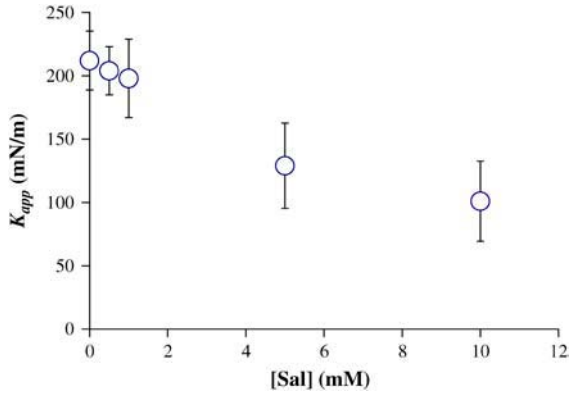

FIGURE 6 The apparent area compressibility (K_{app}) dose-response curve for salicylate-SOPC interaction. Salicylate decreases K_{app} of SOPC vesicles in a dose-dependent manner. The concentrations of salicylate tested were 0 mM, 0.5 mM, 1 mM, 5 mM, and 10 mM. Error bars represent the standard deviation of the mean.

As shown in Fig. 6, 10 mM salicylate decreased K_{app} from ~211 mN/m to ~138 mN/m ($p < 0.05$), a ~40% decrease.

Bending rigidity (k_c) and elastic area compressibility modulus (K_A)

Next, we addressed the issue of whether the changes in K_{app} were due to changes in the bending stiffness (k_c), the elastic area compressibility modulus (K_A), or partitioning. The results of these experiments are shown in Figs. 7 and 8. Salicylate decreased k_c in a dose-dependent manner. The control value of k_c was measured to be $\sim 0.9 \times 10^{-19}$ J, in agreement with earlier measurements for SOPC (21,33). We found that 1 mM salicylate caused a ~40% decrease in k_c to $\sim 0.6 \times 10^{-19}$ J. The K_{app} was only reduced by ~10% from 211 mN/m to 191 mN/m at this same concentration. Higher concentrations of salicylate produced further decreases in k_c, though by a lesser amount than seen at 1 mM. Qualitative evidence for a dramatic change in the bending stiffness comes from observations of clearly apparent thermal fluctuations when the vesicles were suspended in 10 mM salicylate.

Following the methods of Rawicz et al. (33), we removed the contribution of thermal fluctuations and calculated the elastic area compressibility modulus (K_A) of SOPC exposed to salicylate. When the area increase caused by smoothing of the undulations was removed, the K_A of SOPC increased to ~246 mN/m from K_{app} of ~211 mN/m. This value agrees well with the results of Rawicz et al. (33) and Ly et al. (21). Fig. 8 shows salicylate had less effect on K_A at the higher concentrations tested. For example, K_A only decreased ~20% from ~246 mN/m to ~194 mN/m in 10 mM salicylate. Because K_A was calculated from K_{app} by removing the area increase associated with thermal fluctuations, salicylate's small effect on K_A indicates that the significant decrease of K_{app} is mainly due to a decreased bending rigidity that causes induced membrane fluctuations.

We also repeated microaspiration experiments with GUVs formed using the traditional rehydration method in 10 mM

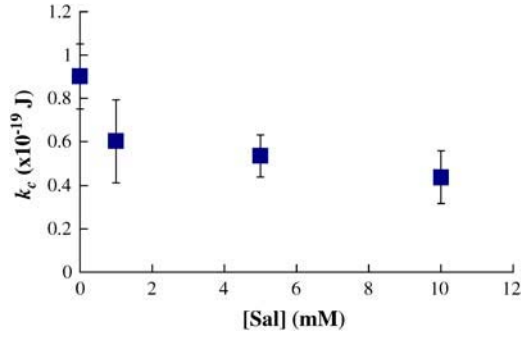

FIGURE 7 A dose-response curve of the effect of salicylate on membrane-bending modulus (k_c) is shown. At low concentrations, salicylate had a dramatic effect on k_c.

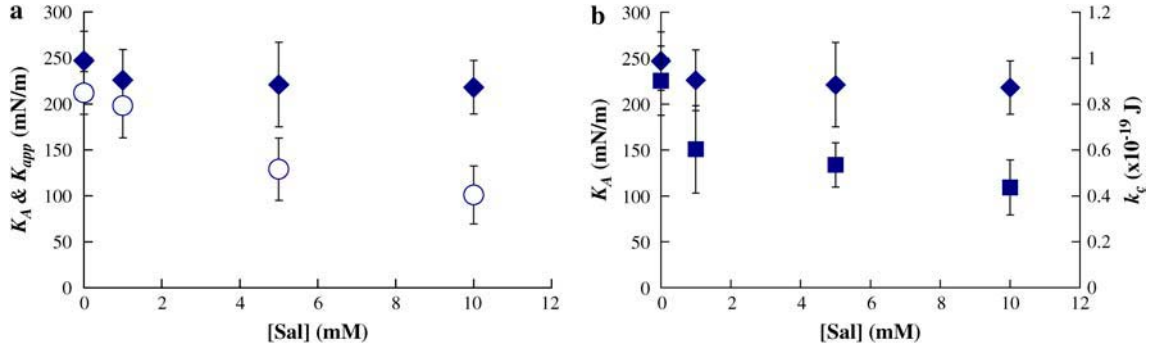

FIGURE 8 (*a*) The effect of salicylate on K_A (♦) compared with K_{app} (○). The K_A curve was obtained by removing the contribution from thermal fluctuations. (*b*) Salicylate's effects on K_A (♦) compared with its effects on the k_c (■).

salicylate. The resulting mechanical parameters showed no statistical difference from those extracted from vesicles made via electroformation (Table 1).

Molecular volume of salicylate in the membrane

To estimate the molecular volume of salicylate, Eq. 5 can be simplified. Assuming that the concentration of salicylate in solution (x_s) is constant because vesicle concentration in the chamber was extremely small (in *p*M) and that measured area increase reflects changes in the salicylate concentration in the membrane, the equation can be derived (22) as

$$\frac{\alpha_{par}}{(x_s)^{n_m/n_s}} = Ce^{\left(\frac{\tau V_{sal}}{l_c\, 2kT}\right)}, \tag{8}$$

where α_{par} is the area dilation caused solely by partition of salicylate molecules at each i^{th} tension level, x_s is the salicylate concentration in solution, and C is a constant. The term of n_m/n_s is an indicator of a change in the state of molecular aggregation during partitioning. The experiments were performed as discussed in Methods, above, to obtain the area increase caused by tension-dependent salicylate partitioning, designated as α_{par}. After the membrane fluctuations were removed, the ln α_{par} versus τ was plotted for 1 mM and 10 mM salicylate (Fig. 9). The slopes of these plots were extrapolated to the tension-free condition to obtain the dependence of $\alpha_{par}(0)$ on the bulk salicylate concentrations (22). The $\alpha_{par}(0)$ values at tension-free state for both 1 mM and 10 mM salicylate were used to calculate the ratio of n_m/n_s that is necessary to deduce the correlation between $\alpha_{par}(0)$ and the bulk salicylate concentration. The n_m/n_s value was estimated to be ~0.5, indicating a pattern of dissociation during insertion. The volume of a salicylate molecule was calculated to be V_{sal} ~240 Å^3 from the slope of the plots in Fig. 9. The estimated molecular volume for methyl salicylate is ~200 Å^3 (44), indicating that our estimated value of V_{sal} is reasonable. Together with the calculated value of n_m/n_s, the molecular volume data imply that salicylate molecules exist as dimers in aqueous solution and dissociate into monomers once in the membrane.

Calculation of the actual elastic compressibility modulus (K_{Ae})

The measured K_A values at each bulk salicylate concentration potentially contain a contribution from the continual partitioning of salicylate into the membrane during aspiration. Although this effect is small—at the lysis tension, an increase of ~5–10% over the initial concentration is expected—it can become significant for surfactants with large packing areas. Because the chemical potential of the solution remains constant when tension in the membrane is changed, Eq. 5 can be written as (21,23)

$$\frac{1}{n_m}\ln\left(\frac{x_{m,o}}{n_m}\right) = \frac{1}{n_m}\ln\left(\frac{x_{m,i}}{n_m}\right) - \frac{\tau}{l_c}\frac{V_{sal}}{2kT}, \tag{9}$$

TABLE 1 Effect of salicylate on membrane mechanical properties of SOPC vesicles

[Sal] (mM)	K_{app} (mN/m)	K_A (mN/m)	k_c (10^{-19} J)	K_{Ae} (mN/m)
0	212 ± 23 (17)	247 ± 32 (7)	0.90 ± 0.15 (10)	247 ± 32 (7)
0.5	204 ± 19 (11)			
1	191 ± 28* (9)	227 ± 41* (9)	0.60 ± 0.19* (6)	235 ± 44 (9)
5	147 ± 33* (23)	200 ± 40* (6)	0.54 ± 0.10* (7)	230 ± 40 (6)
10	138 ± 32* (10)	189 ± 18* (7)	0.44 ± 0.12* (8)	222 ± 16* (7)
SOPC† (rehydration method) 10 mM Sal	128 ± 27 (6)	183 ± 51 (6)	0.45 ± 0.17 (6)	N/A

Values are shown as mean ± SD. The numbers in parentheses represent the number of vesicles used during experiments.
*Values are statistically different from control, as determined by Student's *t*-test results obtained at 95% confidence.
†Experiments with SOPC GUVs synthesized via rehydration method in 10 mM salicylate. There was no statistical difference when compared to parameters extracted from GUVs made using the electroformation method.

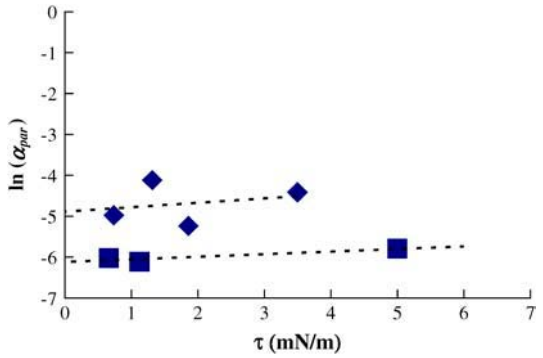

FIGURE 9 Changes in the area dilation as a result of salicylate partitioning at various tension levels. A vesicle was transferred at constant tension levels into known concentrations of salicylate (1 mM, ■, and 10 mM, ♦). Projection-length changes before and after transfer were recorded and used to determine α_{par} as described in the text.

where $x_{m,o}$ is the salicylate concentration in the membrane at zero-tension and $x_{m,i}$ is the membrane salicylate concentration at i^{th} tension. Eq. 9 can be simplified to express the fractional change in the mole fraction of salicylate in the membrane resulting from applied tension,

$$\Delta x_m/x_{m,o} = \exp[V_{sal}\tau/2kTl_c)n_m] - 1, \qquad (10)$$

where $\Delta x_m = x_{m,i} - x_{m,o}$. Since mole fractions of salicylate are considered to be equivalent to the area dilation, α, and $n_m = 1$ as shown above, the above relation can be written as

$$\Delta\alpha_{par}(i) = [\exp(V_{sal}\tau(i)/2kTl_c) - 1]\alpha_{par}(0). \qquad (11)$$

Equation 11 can then be combined with Eqs. 3 and 4 to give the total change-in-area increase that needs to be removed to estimate the true elastic area dilation $\alpha_{Ae}(i) = \alpha_{app}(i) - \Delta\alpha(i)$, where

$$\Delta\alpha(i) = (k_BT/8\pi k_c)\ln[\tau(i)/\tau(1)] + \Delta\alpha_{par}(i). \qquad (12)$$

Using Eqs. 11 and 12, we corrected the area dilation data for all vesicles by removing $\alpha_{par}(i)$ at each tension level. The tension data were then replotted versus α_{Ae} to determine the actual elastic compressibility modulus, designated as K_{Ae}. In practice, this usually resulted in an approximately 10 mN/m increase in the measured compressibility modulus for a given vesicle. This modulus reflects contributions from the initial salicylate partitioning at zero-tension. As shown in Table 1, salicylate was found to have a much smaller effect on K_{Ae} at all concentrations tested after the tension-dependent partitioning was accounted for. The difference between K_{Ae} and K_A is small, but increases with the bulk salicylate concentration, as expected from Eq. 11.

The results of our micromechanical experiments are summarized in Table 1.

Kinetics of salicylate interactions with membranes

Salicylate uptake and recovery curves were obtained using the modified transfer experiment. The vesicle was transferred into the salicylate pipette at a tension of ~1 mN/m and the increase in the projection length was recorded. The fractional area increase (α) was then plotted against time to give the uptake timecourse (Fig. 3). The uptake curve was fitted using the general exponential growth equation, $\alpha = \alpha_o + \alpha_t(1 - e^{k_1 t})$ (OriginLab, Northampton, MA), where α_o is the initial area dilation before the vesicle was exposed to salicylate, α_t is the total increase in α, and k_1 is the time constant of salicylate uptake. The recovery curve was fitted with the standard exponential decay function $\alpha = \alpha_o + Ae^{-k_2 t}$, where A is an arbitrary parameter and k_2 is the time constant of salicylate recovery. For the experiment shown in Fig. 3, k_1 was ~0.5 ± 0.06 s^{-1} and k_2 was ~0.15 ± 0.08 s^{-1}. The time for equilibration of salicylate with the membrane is much faster than that reported for the lysolipid mono-oleoylphosphatidylcholine, where $k_1 = 0.3$ s^{-1} (23) and for the uptake of bile acids, which require up to ~30 s to reach equilibrium (22).

Dynamic tension spectroscopy

To test the effect of salicylate on membrane strength, we performed dynamic tension spectroscopy (DTS). We verified results obtained by Evans et al. (31) in control conditions and performed experiments in 10 mM salicylate. A total of 120 vesicles were used.

As Fig. 10 shows, 10 mM salicylate clearly shifted the DTS spectrum of an SOPC membrane. The effects were most dramatic in the low-tension domain that represents the cavitation process. The application of 10 mM salicylate reduced σ_c to ~50 mN/m from the control value of ~129 mN/m and reduced ν_c to ~1×10^5 s^{-1} from the control value of ~1×10^6 s^{-1}. In the high-tension domain the effects were not as dramatic: σ_δ was practically unchanged in 10 mM salicylate, and ν_δ showed a modest increase from

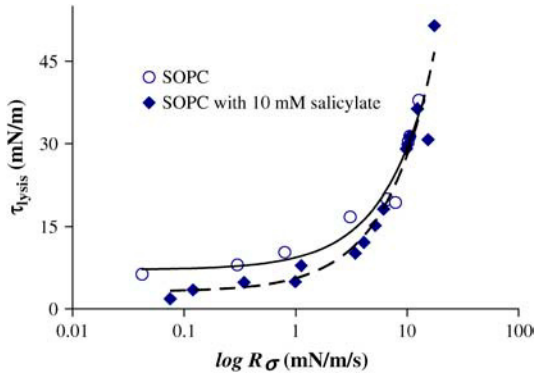

FIGURE 10 Dynamic tension spectra (*DTS*) of SOPC in 200 mM glucose (○) and SOPC with 10 mM salicylate (♦). The solid and dashed lines represent the trends of the data. Salicylate does not affect σ_δ in the high-tension regime at this concentration. However, σ_c in the low-tension regime was shifted down from ~160 mN/m (SOPC) to ~51 mN/m with 10 mM salicylate.

TABLE 2 Dynamic tension measurements

Dynamic tension properties	σ_δ (mN/m)	ν_δ (s^{-1})	σ_c (mN/m)	ν_c(s^{-1})	ε (pJ/m)
SOPC	3.2	0.32	129	1×10^6	14.2
SOPC + 10 mM salicylate	3.3	0.98	51	1×10^5	7.9

0.32 s^{-1} to 0.98 s^{-1}. The results of the DTS experiments are summarized in Table 2. The shift of the spectrum demonstrates that salicylate increases the frequency of spontaneous defects and also affects membrane strength by lowering the energy barrier of hole formation, hence stabilizing membrane holes.

The tension scale of cavitation formation is dependent upon the edge energy of the unstable cavity, which can be expressed as $\sigma_c = \pi\varepsilon^2/k_BT$, where ε is the membrane edge energy (31). The ε-values of both pure SOPC and SOPC with 10 mM salicylate were calculated and listed in the Table 2 along with tension scale and frequency data. The results indicate that the membrane edge energy was significantly lowered in the presence of salicylate.

DISCUSSION

The underlying mechanisms responsible for the diverse biological effects of salicylate and other NSAIDs are a matter of considerable controversy in the literature. Some maintain that these drugs exert all their biological effects, including therapeutic functions and side effects, as a result of direct interactions with enzymes, such as COX (2,3). However, others assert NSAIDs' side effects are actually caused by nonspecific interactions with biomembranes (1,6,11,45). It should be noted that in Vane's classic article, it was reported that salicylate, which has profound anti-inflammatory activity, was the least potent of the NSAIDs in inhibiting prostaglandin biosynthesis (3), providing evidence for a non-COX-mediated mechanism of action of salicylate and perhaps other drugs of this class. Here, we have demonstrated that physiological concentrations of salicylate can have dramatic effects on the mechanical properties of an SOPC membrane.

Salicylate decreases membrane bending rigidity

One very important point we have established is that salicylate decreases membrane strength by affecting molecular processes associated with the formation of both defects and holes. Often in the biophysical literature the term ''pores'' is used to designate transport pathways across the membrane without reference to a two-state model of membrane rupture. Since the formation of membrane pores is believed to govern the passive permeability of membranes (46) and plays an important part in phospholipid translocation (47,48), these results imply that salicylate alters the membrane's hydrophobic barrier properties. In particular, we have found that salicylate increases the frequency of occurrence of spontaneous defects. Moreover, salicylate significantly lowers the tension scale of cavitation formation, but leaves the tension scale of defect formation unaffected, indicating that salicylate stabilizes membrane holes without disrupting lipid cohesion. Salicylate's small effect on the defect process agrees with our membrane elasticity results, which demonstrate that salicylate does not significantly decrease the actual elastic compressibility modulus at the concentrations tested. The large downshift in the low-tension domain (related to hole formation) of the DTS spectrum in the presence of salicylate is consistent with our measurements, which show that salicylate decreases membrane bending stiffness, thereby stabilizing holes. The demonstrated decrease in the edge energy of a hole when the membrane was exposed to salicylate (Table 2) provides further support for this argument. In Fig. 11, we demonstrate that our data correlates well with the ε-versus-k_c data that Evans et al. (31) presented for membranes composed of lipids with different chain length and unsaturation levels. Therefore, both the elasticity and dynamic tension results coincide to show that by lowering the bending stiffness, salicylate stabilizes membrane holes, causing a weaker and likely a more permeable membrane.

The bending and area compressibility moduli of a thin material are related to each other by the relationship $k_c = K_{Ae}h_m^2/c$, where h_m is the thickness of the monolayer and c is a constant (33). The result that salicylate has a large effect on k_c and a lesser effect on K_{Ae} suggests that salicylate changes the thickness of the membrane. In Fig. 12, the plot $(k_c/K_{Ae})^{1/2}$ versus [Sal] shows that our data are consistent with a dose-dependent thinning of the membrane. We have measured the effect of salicylate on the height of supported monolayers using atomic force microscopy, and our preliminary

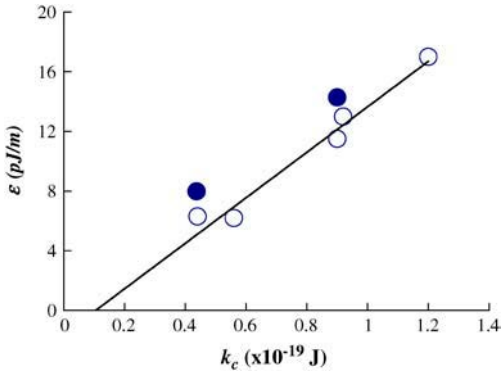

FIGURE 11 The correlation between edge energy of the hole and membrane-bending stiffness. The data points of ε versus k_c for salicylate (●) were superimposed onto the ε-versus-k_c plot that Evans et al. (31) obtained for membranes composed of lipids with different chain length and unsaturation levels (○).

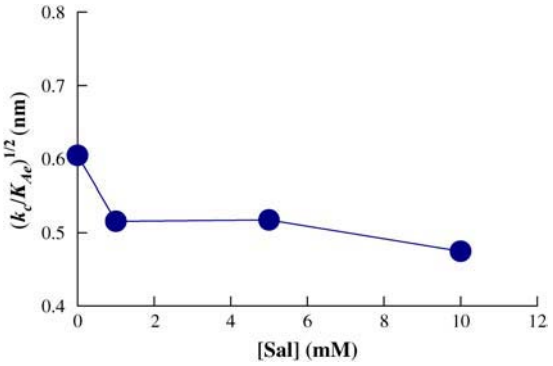

FIGURE 12 Predicted change in bilayer thickness, $(k_c/K_{Ae})^{1/2}$, as result of salicylate incorporation. The estimated changes using experimentally determined values of K_{Ae} and k_c at different salicylate concentrations are consistent with a salicylate-induced thinning of the membrane. The line is used to indicate the trend.

observations indicate a noticeable thinning of the membrane in the presence of 5 mM salicylate (data not shown).

Interestingly, membranes composed of PC lipids with acyl chains ranging from 13 to 22 carbons and containing up to two double bonds all have a similar K_A, but k_c varies widely among these membranes; these observations are explained by changes in membrane thickness (33). Coupled with the correlation shown in Fig. 12, these observations suggest that incorporation of salicylate into a PC membrane makes its properties similar to those of a membrane composed of shorter chain and/or polyunsaturated lipids. It is also interesting to note that certain peptides, such as the antimicrobial peptide alamethicin, can also induce pore formation by thinning the membrane and then preferentially inserting into the edges of the membrane pores (49–51). Moreover, alamethicin-induced membrane thinning reaches a plateau when the peptide/lipid ratio becomes larger than a critical value (49), similar to the trend predicted for salicylate (Fig. 12). These considerations emphasize that the correlation between membrane thinning and peptide-induced pore formation reflect an underlying general biophysical mechanism.

Free energy of transfer and partition coefficient

The Gibbs free energy of salicylate adsorption into the membrane can be estimated from our experimental data using a thermodynamic expression well developed for monolayers (52) and recently applied to bilayers (21),

$$\Delta G_t^0 = -RT \ln(d\Delta\gamma/dc)_{c\to 0}, \qquad (13)$$

where ΔG_t^0 is the change in free energy associated with the transfer of salicylate from water into the SOPC membrane. The term $(d\Delta\gamma/dc)$ represents the change in surface tension as salicylate concentration changes. This term can be estimated by relating the actual compressibility modulus K_{Ae} to the surface pressure Π and recalling that surface tension is equal to surface pressure ($\gamma = \Pi$) at the stress-free state (21). Using an idealized polymer-brush model of membrane elasticity, Rawicz et al. (33) predicted that $K_{Ae} \sim 6\Pi$, and thus $\gamma \sim K_{Ae}/6$. Based on our data, ΔG_t^0 for salicylate partitioning into the membrane is $\sim -13.5 \pm 3.9$ kJ/mol. However, this value should be viewed with caution; although we measured a change in K_{Ae} with salicylate concentrations lower than 10 mM, a rigorous *t*-test did not indicate our values were significant at 95% level.

Because of the structural similarities between salicylate and benzoic acid, the thermodynamics of salicylate's interaction with the membrane may be comparable to that of benzoic acid. The free energy of hydration (ΔG_w^0) of benzoic acid at 25°C is ~ -16 kJ/mol, and its free energy of solvation in *n*-octanol (ΔG_{oct}^0) is ~ -30 kJ/mol, and so its free energy of transfer is $\Delta G_t^0 = \Delta G_{oct}^0 - \Delta G_w^0 = \sim -15\,\mathrm{kJ/mol}$ (53). This implies that hydrophobic effects play an important role in salicylate partitioning into the membrane. The difference may arise from the fact that salicylate, with a pK_a of ~3, would exist predominantly as an anion in a nearly neutral solution, which can have unfavorable electrostatic interactions with lipids. Furthermore, the additional hydroxyl group on salicylate may lead to more favorable interactions with the aqueous solution, thus further decreasing ΔG_t^0.

The change in free energy of adsorption can be used to compute the partition coefficient P_{mem} from the standard relationship $P_{mem} = e^{-\Delta G_t^0/RT}$. Our value of ΔG_t^0 corresponds to a log (P_{mem}) ~2.1. To our knowledge, we are the first to measure the partition coefficient of salicylate into a biological membrane. However, the partition coefficient for sodium salicylate into an octanol/water interface has been reported to be log(P_{oct}) ~1.5 (54). A recent study reports that partition coefficients for weak organic acids such as salicylate, estimated using octanol-water interfaces (P_{oct}), are generally underestimates of partition coefficients (P_{mem}) into biological membranes (55). Notably at pH 6 where our experiments were performed, the difference between P_{mem} and P_{oct} can be approximately an order of magnitude. Thus, our reported partition coefficient agrees with the literature value once this correction is taken into account, which reinforces the accuracy of our estimated value of ΔG_t^0.

From the transfer experiment, it is tempting to argue that the time constants for salicylate uptake and recovery represent salicylate adsorption and desorption from the membrane. However, it is easy to illustrate that this assumption gives incorrect results. Assuming $K_{eq} = k_1/k_2$, the equilibrium constant, K_{eq}, is $\sim 3.3 \pm 1.8$. The relationship $\Delta G^{ads} = -RT\ln K_{eq}$ then gives ΔG^{ads} ~3 kJ/mol, and the corresponding log (P_{mem}) of ~0.5. These values are clearly too small compared to the literature value of 1.5 for log (P_{mem}) (54). Thus, the experimentally observed time constants are not indicative of adsorption and desorption processes, but likely also reflect flip-flop and bilayer crossing.

The molecular area and volume of salicylate in an SOPC membrane

The estimated salicylate volume of ~240 Å^3 in the membrane is equivalent to the physical size of one salicylate molecule and corresponds to an estimated cross-sectional area of ~50 Å^2. Since the aromatic ring occupies most of the physical space in a salicylate molecule, benzene can be used for comparison in terms of packing. The cross-sectional area of benzene varies between ~22 Å^2 and ~69 Å^2, depending on the absorbent (56). The packing area of salicylate is between that of bile acids (60 Å^2) (22) and lysolipids (35 Å^2) (23). However, the interactions of salicylate with the membrane are significantly different. Whereas both bile acids and lysolipids had large effects on membrane elasticity, salicylate showed a small effect on the elastic compressibility. The difference may arise from the finding that salicylate occupies much less volume (~240 Å^3) in the membrane than bile acids and lysolipids (between 1000 Å^3 and 2000 Å^3). Therefore, molecular volume becomes an important factor in ascertaining the effects of small molecules on membrane elasticity.

Our results that the value of n_m/n_s is ~0.5 are consistent with salicylate forming dimers in solution. The idea of salicylate forming dimers in solution is not unusual, since the carboxyl and hydroxyl groups covalently attached on salicylate's aromatic ring can participate in H-bonding with those on the adjacent molecule(s) and establish a dimeric form in solution. There is evidence that salicylate molecules exist as dimers in solution (25), which is purported to explain salicylate's ability to induce micellar chain formation (26). In this NMR study, salicylate molecules in one micelle were shown to form dimers with salicylate molecules in the membranes of neighboring micelles.

Salicylate's membrane-mediated biological activity

Long-term consumption of non-steroidal anti-inflammatory drugs (NSAIDs), such as aspirin and salicylate, can lead to undesirable side effects that have serious consequences. Side effects such as gastric intestinal (GI) toxicity are related to the ability of these drugs to interact with the membrane (5,45,57,58). Salicylate and other NSAIDs decrease the hydrophobicity of the membrane layer covering the gastric mucosa, causing the membrane to become more wettable (10,45,57,59,60). The detailed structure of the phospholipid layer covering the GI mucosa is unknown, but the characteristic structure of the GI tract is rugae and pits (61), both of which are highly curved structures. Because salicylate is effective at decreasing membrane bending stiffness, it is likely to disrupt the structural integrity of the phospholipid layer in the GI tract as well as perhaps leading to cavitation formation.

Another non-COX-mediated effect of salicylate is on hearing. The mechanism by which salicylate affects hearing is due to the ability of salicylate to attenuate outer hair cell electromotility (62,63). Some argue that salicylate affects the function of the outer hair cell motor protein prestin by competing with chloride ions for putative binding sites on the molecule (64). However, the growing recognition that protein conformational changes are associated with changes in membrane curvature and mechanical properties (24,65) suggests the possibility that salicylate's ability to dramatically decrease k_c may be involved in its effects on electromotility. This interpretation is consistent with the membrane-bending model of electromotility, which proposes that electrically induced changes in nanoscale membrane curvature are involved in electromotility (66).

Finally, it is speculated that salicylate increases the water permeability of biomembranes, including the outer hair cell plasma membrane, by inducing the formation of membrane pores (67). Our DTS finding supports this argument because salicylate acts to lower the energy barrier for forming membrane cavitations, thereby leading to a stabilization of the membrane holes.

CONCLUSION

As a powerful NSAID, salicylate has been used since ancient times to treat a series of inflammatory responses, such as fever, pain, and arthritis. However, NSAIDs, including salicylate, cause serious side effects. The cause of these side effects is a subject of active debate, with some advocating specific drug-enzyme interactions and other arguing for nonspecific drug-membrane interactions. Here, through mechanical studies of micropipette aspiration and dynamic tension spectroscopy, we have demonstrated that salicylate interacts with lecithin membranes and changes their mechanical properties at physiological concentrations. Membranes containing salicylate have lowered bending stiffness, rupture more easily, and are likely to be thinner and more permeable. These mechanical changes induced by salicylate may affect several physiological processes, especially those mediated by membrane proteins.

We are grateful to Drs. Lenard Lichtenberger and Huey Huang for insightful discussions and for critiquing a draft of this manuscript. We also thank Dr. Robert Cantor for pointing out important references on surfactant partitioning into bilayer membranes.

This study was supported in part by a grant from the state of Texas Technology Development and Transfer Program.

REFERENCES

1. Weissmann, G. 1991. Aspirin. *Sci. Am.* 264:84–90.
2. Vane, J. R., Y. S. Bakhle, and R. M. Botting. 1998. Cyclooxgenases 1 and 2. *Annu. Rev. Pharmacol. Toxicol.* 38:97–120.
3. Vane, J. R. 1971. Inhibition of prostaglandin synthesis as a mechanism of action for aspirin-like drugs. *Nat. New Biol.* 231:232–235.
4. Weissmann, G., M. C. Montesinos, M. Pillinger, and B. N. Cronstein. 2002. Non-prostaglandin effects of aspirin III and salicylate: inhibition

of integrin-dependent human neutrophil aggregation and inflammation in COX 2- and NF-κ-B (P105)-knockout mice. *Adv. Exp. Med. Biol.* 507:571–577.

5. Wallace, J. L. 1997. Nonsteroidal anti-inflammatory drugs and gastroenteropathy: the second hundred years. *Gastroenterology.* 112: 1000–1016.
6. Lichtenberger, L. M. 2001. Where is the evidence that cyclooxygenase inhibition is the primary cause of nonsteroidal anti-inflammatory drug (NSAID)-induced gastrointestinal injury? Topical injury revisited. *Biochem. Pharmacol.* 61:631–637.
7. Myers, E. N., and J. M. Bernstein. 1965. Salicylate ototoxicity; a clinical and experimental study. *Arch. Otolaryngol.* 82:483–493.
8. Jung, T. T., C. K. Rhee, C. S. Lee, Y. S. Park, and D. C. Choi. 1993. Ototoxicity of salicylate, nonsteroidal antiinflammatory drugs, and quinine. *Otolaryngol. Clin. North Am.* 26:791–810.
9. Ligumsky, M., E. M. Golanska, D. G. Hansen, and G. L. Kauffman, Jr. 1983. Aspirin can inhibit gastric mucosal cyclo-oxygenase without causing lesions in Rat. *Gastroenterology.* 84:756–761.
10. Lichtenberger, L. M. 1995. The hydrophobic barrier properties of gastrointestinal mucus. *Annu. Rev. Physiol.* 57:565–583.
11. Lichtenberger, L. M., Z. M. Wang, J. J. Romero, C. Ulloa, J. C. Perez, M. N. Giraud, and J. C. Barreto. 1995. Non-steroidal anti-inflammatory drugs (NSAIDs) associate with Zwitterionic phospholipids: insight into the mechanism and reversal of NSAID-induced gastrointestinal injury. *Nat. Med.* 1:154–158.
12. Goddard, P. J., B. A. Hills, and L. M. Lichtenberger. 1987. Does aspirin damage canine gastric mucosa by reducing its surface hydrophobicity? *Am. J. Physiol.* 252:G421–G430.
13. Goddard, P. J., Y. C. Kao, and L. M. Lichtenberger. 1990. Luminal surface hydrophobicity of canine gastric mucosa is dependent on a surface mucous gel. *Gastroenterology.* 98:361–370.
14. Lundbaek, J. A., P. Birn, A. J. Hansen, R. Sogaard, C. Nielsen, J. Girshman, M. J. Bruno, S. E. Tape, J. Egebjerg, D. V. Greathouse, G. L. Mattice, R. E. Koeppe II, et al. 2004. Regulation of sodium channel function by bilayer elasticity: the importance of hydrophobic coupling. Effects of micelle-forming amphiphiles and cholesterol. *J. Gen. Physiol.* 123:599–621.
15. Gennis, R. B. 1989. Biomembrane-Molecular Structure and Function. C. R. Cantor, editor. Springer-Verlag, New York.
16. Cevc, G., and D. Marsh. 1987. Phospholipid Bilayers: Physical Principles and Models. E.E. Bittar, editor. John Wiley & Sons, New York.
17. Evans, E. A., and R. Skalak. 1980. Mechanics and Thermodynamics of Biomembranes. CRC Press, Boca Raton, FL.
18. Israelachvili, J. N., D. J. Mitchell, and B. W. Ninham. 1976. Theory of self-assembly of hydrocarbon amphiphiles into micelles and bilayers. *J. Chem. Soc. Faraday Trans. II.* 72:1525–1568.
19. Israelachvili, J. N., S. Marcelja, and R. G. Horn. 1980. Physical principles of membrane organization. *Q. Rev. Biophys.* 13:121–200.
20. Hung, V. L., D. E. Block, and M. L. Longo. 2002. Interfacial tension effect of ethanol on lipid bilayer rigidity, stability, and area/molecule: a micropipette aspiration approach. *Langmuir.* 18:8988–8995.
21. Ly, H. V., and M. L. Longo. 2004. The influence of short-chain alcohols on interfacial tension, mechanical properties, area/molecule, and permeability of fluid lipid bilayers. *Biophys. J.* 87:1013–1033.
22. Evans, E. A., W. Rawicz, and A. Hoffmann. 1995. Lipid bilayer expansion and mechanical disruption in solutions of water-soluble bile acid. *In* Bile Acids in Gastroenterology: Basic and Clinical Advances. A. Hoffmann, G. Paumgartner, and A. Stiehl, editors. Kluwer Academic, Boston, MA.
23. Zhelev, D. V. 1998. Material property characteristics for lipid bilayers containing lysolipid. *Biophys. J.* 75:321–330.
24. Cantor, R. S. 1999. Lipid composition and the lateral pressure profile in bilayers. *Biophys. J.* 76:2625–2639.
25. Stein, G. T. M. 1969. Report NYO-3242–30. U.S. Atomic Energy Commission, Washington, DC.
26. Rao, U. R., C. Manohar, B. S. Valaulikar, and R. M. Iyer. 1987. Micellar chain model for the origin of the viscoelasticity in dilute surfactant solutions. *J. Phys. Chem.* 91:3286–3291.
27. Troiano, G. C., K. J. Stebe, R. M. Raphael, and L. Tung. 1999. The effects of gramicidin on electroporation of lipid bilayers. *Biophys. J.* 76:3150–3157.
28. Angelova, M. J., S. Soleau, P. Melaeard, J. F. Faucon, and P. Bothorel. 1992. Preparation of giant vesicles by AC electric fields. Kinetics and applications. *Prog. Colloid Polym. Sci.* 89:127–131.
29. Needham, D., and R. S. Nunn. 1990. Elastic deformation and failure of lipid bilayer membranes containing cholesterol. *Biophys. J.* 58: 997–1009.
30. Shoemaker, S. D., and T. K. Vanderlick. 2002. Intramembrane electrostatic interactions destabilize lipid vesicles. *Biophys. J.* 83: 2007–2014.
31. Evans, E., V. Heinrich, F. Ludwig, and W. Rawicz. 2003. Dynamic tension spectroscopy and strength of biomembranes. *Biophys. J.* 85: 2342–2350.
32. Kwok, R., and E. Evans. 1981. Thermoelasticity of large lecithin bilayer vesicles. *Biophys. J.* 35:637–652.
33. Rawicz, W., K. C. Olbrich, T. McIntosh, D. Needham, and E. Evans. 2000. Effect of chain length and unsaturation on elasticity of lipid bilayers. *Biophys. J.* 79:328–339.
34. Evans, E., and W. Rawicz. 1990. Entropy-driven tension and bending elasticity in condensed-fluid membranes. *Phys. Rev. Lett.* 64: 2094–2097.
35. Schneider, M. B., J. T. Jenkins, and W. W. Webb. 1984. Thermal fluctuations of large cylindrical phospholipid vesicles. *Biophys. J.* 45:891–899.
36. Needham, D., and D. V. Zhelev. 1995. Lysolipid exchange with lipid vesicle membranes. *Ann. Biomed. Eng.* 23:287–298.
37. Olbrich, K., W. Rawicz, D. Needham, and E. Evans. 2000. Water permeability and mechanical strength of polyunsaturated lipid bilayers. *Biophys. J.* 79:321–327.
38. Mui, B. L., P. R. Cullis, E. A. Evans, and T. D. Madden. 1993. Osmotic properties of large unilamellar vesicles prepared by extrusion. *Biophys. J.* 64:443–453.
39. Evans, E. A., R. Waugh, and L. Melnik. 1976. Elastic area compressibility modulus of red cell membrane. *Biophys. J.* 16:585–595.
40. Wu, Y., and G. L. Fletcher. 2000. Efficacy of antifreeze protein types in protecting liposome membrane integrity depends on phospholipid class. *Biochim. Biophys. Acta.* 1524:11–16.
41. Saleh, A. M., A. T. Florence, T. L. Whateley, and L. K. el-Khordagui. 1989. The effect of hydrotropic agents on the heat coagulation of bovine serum albumin. *J. Pharm. Pharmacol.* 41:298–301.
42. Sue, Y. J., and M. Shannon. 1992. Pharmacokinetics of drugs in overdose. *Clin. Pharmacokinet.* 23:93–105.
43. Pena-Alonso, Y. R., M. A. Montoya-Cabrera, E. Bustos-Cordoba, L. Marroquin-Yanez, and V. Olivar-Lopez. 2003. Aspirin intoxication in a child associated with myocardial necrosis: is this a drug-related lesion? *Pediatr. Dev. Pathol.* 6:342–347.
44. Marcus, Y. 1985. Ion Solvation. John Wiley & Sons, London, UK.
45. Lichtenberger, L. M., C. Ulloa, A. L. Vanous, J. J. Romero, E. J. Dial, P. A. Illich, and E. T. Walters. 1996. Zwitterionic phospholipids enhance aspirin's therapeutic activity, as demonstrated in rodent model systems. *J. Pharmacol. Exp. Ther.* 277:1221–1227.
46. Monnard, P. A., and D. W. Deamer. 2001. Nutrient uptake by protocells: a liposome model system. *Orig. Life Evol. Biosph.* 31:147–155.
47. Raphael, R. M., and R. E. Waugh. 1996. Accelerated interleaflet transport of phosphatidylcholine molecules in membranes under deformation. *Biophys. J.* 71:1374–1388.
48. Raphael, R. M., R. E. Waugh, S. Svetina, and B. Zeks. 2001. Fractional occurrence of defects in membranes and mechanically driven interleaflet phospholipid transport. *Phys. Rev. E Stat. Nonlin. Soft Matter Phys.* 64:051913.

49. Chen, F. Y., M. T. Lee, and H. W. Huang. 2003. Evidence for membrane thinning effect as the mechanism for peptide-induced pore formation. *Biophys. J.* 84:3751–3758.

50. Lee, M. T., F. Y. Chen, and H. W. Huang. 2004. Energetics of pore formation induced by membrane active peptides. *Biochemistry.* 43: 3590–3599.

51. Huang, H. W., F. Y. Chen, and M. T. Lee. 2004. Molecular mechanism of peptide-induced pores in membranes. *Phys. Rev. Lett.* 92:198304.

52. Heywang, C., G. Mathe, D. Hess, and E. Sackmann. 2001. Interaction of GM(1) glycolipid in phospholipid monolayers with wheat germ agglutinin: effect of phospholipidic environment and subphase. *Chem. Phys. Lipids.* 113:41–53.

53. Perlovich, G. L., S. V. Kurkov, A. N. Kinchin, and A. Bauer-Brandl. 2003. Thermodynamics of solutions. IV. Solvation of ketoprofen in comparison with other NSAIDs. *J. Pharm. Sci.* 92:2502–2511.

54. Drayton, C. J. 1990. Cumulative subject index and drug compendium. *In* Comprehensive Medicinal Chemistry. P.G.S.C. Hansch and J.B. Taylor, editors. Pergamon Press, Oxford, UK.

55. Escher, B. I., and R. P. Schwarzenbach. 2002. Mechanistic studies on baseline toxicity and uncoupling of organic compounds as a basis for modeling effective membrane concentrations in aquatic organisms. *Aquat. Sci.* 64:20–35.

56. McClellan, A. L., and A. H. F. Harnsberger. 1967. Cross-sectional areas of molecules adsorbed on solid surfaces. *J. Colloid Interface Sci.* 23:577–599.

57. Morris, G. P., J. L. Wallace, P. L. Harding, E. J. Krausse, and S. J. Lolle. 1984. Correlations between changes in indicators of gastric mucosal barrier integrity at time of exposure to ''barrier breakers'' and extent of hemorrhagic erosions one hour later. *Dig. Dis. Sci.* 29: 6–11.

58. Abramson, S., and G. Weissmann. 1989. The mechanisms of action of nonsteroidal antiinflammatory drugs. *Clin. Exp. Rheumatol.* 7(Suppl 3): S163–S170.

59. Kao, Y. C., P. J. Goddard, and L. M. Lichtenberger. 1990. Morphological effects of aspirin and prostaglandin on the canine gastric mucosal surface. Analysis with a phospholipid-selective cytochemical stain. *Gastroenterology.* 98:592–606.

60. Giraud, M. N., C. Motta, J. J. Romero, G. Bommelaer, and L. M. Lichtenberger. 1999. Interaction of indomethacin and naproxen with gastric surface-active phospholipids: a possible mechanism for the gastric toxicity of nonsteroidal anti-inflammatory drugs (NSAIDs). *Biochem. Pharmacol.* 57:247–254.

61. Siew, S., and M. L. Goldstein. 1981. Scanning electron microscopy of mucosal biopsies of the human upper gastrointestinal tract. *Scan. Electron Microsc.* 4:173–181.

62. Kakehata, S., and J. Santos-Sacchi. 1996. Effects of salicylate and lanthanides on outer hair cell motility and associated gating charge. *J. Neurosci.* 16:4881–4889.

63. Shehata, W., E. Brownell, and R. Dieler. 1991. Effects of salicylate on shape, electromotility and membrane characteristics of isolated outer hair cells from guinea pig cochlea. *Acta Otolaryngol.* 111:707–718.

64. Oliver, D., D. Z. He, N. Klocker, J. Ludwig, U. Schulte, S. Waldegger, J. P. Ruppersberg, P. Dallos, and B. Fakler. 2001. Intracellular anions as the voltage sensor of prestin, the outer hair cell motor protein. *Science.* 292:2340–2343.

65. Gov, N., and S. A. Safran. 2004. Pinning of fluid membranes by periodic harmonic potentials. *Phys. Rev. E Stat. Nonlin. Soft Matter Phys.* 69:011101.

66. Raphael, R. M., A. S. Popel, and W. E. Brownell. 2000. A membrane bending model of outer hair cell electromotility. *Biophys. J.* 78: 2844–2862.

67. Morimoto, N., R. M. Raphael, A. Nygren, and W. E. Brownell. 2002. Excess plasma membrane and effects of ionic amphipaths on mechanics of outer hair cell lateral wall. *Am. J. Physiol. Cell Physiol.* 282:C1076–C1086.